論文 / 著書情報
Article / Book Information

Title	Thermal barrier coating made of porous zirconium oxide on a nickel-based single crystal superalloy formed by plasma electrolytic oxidation
Author	TAKASHI AKATSU, Takashiro KATO, Yutaka SHINODA, Fumihiro WAKAI
Journal/Book name	Surface & Coatings Technology, Volume 223, No. 25, p. 47-51
Issue date	2013, 2
URL	http://www.journals.elsevier.com/surface-and-coatings-technology/
DOI	http://dx.doi.org/10.1016/j.surfcoat.2013.02.026
Note	このファイルは著者（最終）版です。 This file is author (final) version.

Thermal barrier coating made of porous zirconium oxide on a nickel-based single crystal superalloy formed by plasma electrolytic oxidation

T. Akatsu*, T. Kato, Y. Shinoda, F. Wakai

Secure Materials Center, Materials and Structures Laboratory, Tokyo Institute of Technology, R3-24, 4259 Nagatsuta, Midori, Yokohama 226-8503, Japan

Abstract

A thermal barrier coating (TBC) made of porous ZrO_2 ceramic was formed on a nickel-based single crystal superalloy (NSA) by plasma electrolytic oxidation (PEO). An oxidation barrier coating (OBC) made of Al_2O_3 based ceramics was created between the TBC and NSA substrate by coating the NSA with aluminum before the PEO treatment that oxidized it into Al_2O_3. The key finding of this study is that ZrO_2-based TBC can be formed by PEO of an OBC-coated NSA in a $K_2[Zr(CO_3)_2(OH)_2]$ solution. The TBC contained monoclinic-, tetragonal- and cubic-ZrO_2 crystals and had a unique gradient porous texture. Relatively large pores existed near the interface between OBC and TBC, and the number and size of pores in the TBC decreased with increasing distance from the interface. The TBC had ZrO_2 grains with a diameter of about 300 nm. The TBC shows a low thermal conductivity equivalent to that of conventional TBCs owing to this porous texture with fine grains. The bond strength between the PEO coating and substrate was 26.8±6.6 MPa, which is close to that of conventional TBCs.

Keywords

Thermal barrier coating, Thermal conductivity, Bond strength, Porous material, Plasma electrolytic oxidation, Zirconia, Nickel based single crystal superalloy

*Corresponding author
Tel: +81-45-924-5336
E-mail: akatsu.t.aa@m.titech.ac.jp

1. Introduction

In an effort to reduce fuel consumption and CO_2 emissions, jet and gas turbine engines are being made more thermally efficient by increasing their inlet temperatures. Those temperatures, however, exceeded the melting point of turbine blades made of nickel based single crystal superalloy (NSA), and as a result, such blades are being coated with porous ZrO_2 as a thermal barrier and cooled by air flow.

The thermal barrier coating (TBC) made of ZrO_2 is formed by electron beam physical vapor deposition (EB-PVD) [1] or air plasma spray (APS) [2]. The TBCs made with these techniques are, however, very expensive. In addition, it seems to be rather difficult to use these vapor processing techniques to make TBCs on large components with complex shapes.

Plasma electrolytic oxidation (PEO) is characterized by spark discharges or electrical micro arcs. In the PEO process, high voltage is applied between an anode target metal and a cathode in an electrolytic solution. PEO is a liquid process and is, in principle, able to be used to coat large components with a complex shapes [3]. It has another advantage for TBCs in that it can easily make porous coatings because breakdown with the spark discharges naturally create pores extended in the direction of coating thickness in the coating.

The authors have reported on the fabrication of ZrO_2-based porous ceramic coatings on NSAs with the PEO technique [4]. Other studies on using PEO to make ZrO_2-based ceramic coatings have been done on surface modification of aluminium and magnesium alloys to enhance wear or corrosion resistance [5-24]. The ZrO_2 on these alloys were formed by using electrolytes containing potassium fluorozirconate (K_2ZrF_6) additive [5-22]. However, PEO with K_2ZrF_6 produces fluoride, which is chemically unstable at elevated temperatures; hence, it seems to be an unsuitable way to make TBCs [5-22].

A key finding of our previous study was that performing PEO on NSA in a $K_2[Zr(CO_3)_2(OH)_2]$ solution can produce a good ZrO_2 coating [4]. The ZrO_2 coating was formed by oxidation at the anode surface, in which Zr^{4+} ions from the electrolyte were incorporated in the coating. In the current paper, we describe the processing and characterization of ZrO_2-based TBC made by PEO. The important properties of the TBC are examined, especially the bond strength between the TBC and NSA substrate, and the thermal conductivity. These properties are compared with those of conventional coatings to see if PEO is a practical way of fabricating TBCs. The forming mechanism of the PEO coating is discussed in relation to its properties and microstructure.

2. Experimental procedures

2.1. Fabrication of thermal barrier coating on a nickel based single crystal superalloy through plasma electrolytic oxidation

The NSA used in this study had the chemical composition 5.6Al-9Co-6.5Cr-0.6Mo-6.5Ta-1Ti-6W-3Re-bal.Ni in weight percentage (it is called CMSX-4).

ZrO_2 has a large oxygen diffusion coefficient intrinsically. In addition, the ZrO_2 coating is porous, which causes it to have very low thermal conductivity, and it cannot prevent oxygen in the ambient from diffusing to the substrate underneath. The resulting oxidation caused by the rapid rate of oxygen diffusion severely degrades the substrate at elevated temperatures. For this reason, an oxidation barrier coating (OBC) should be placed between the TBC and the NSA substrate. An OBC made of Al_2O_3 can suppress oxidation because its oxygen diffusion coefficient is very small (~$10^{-12}$$cm^2$/sec at 1400$^oC$) and Al_2O_3 is stable at elevated temperatures. In the conventional coating method, high-temperature oxidation of the CoNiCrAlY alloy bond coating between the TBC and NSA substrate prevents oxidation of the substrate by generating a thermal grown oxide (TGO) layer made of Al_2O_3 ceramic on its surface [25].

In this study, the NSA substrate was coated with aluminum before the PEO treatment that oxidized it to form the Al_2O_3 based OBC. The NSA substrate was soaked

in NaOH solution for 10 min and followed by soaking in HCl solution for 5 min before aluminum coating. The coating was made by dipping the NSA substrate into an aluminium melt at 705^{o}C for 3 minutes. The NSA coated with aluminum was soaked in HNO_3 solution for 1 min after aluminum coating. The coated substrate and an isotropic graphite plate were used as the anode and the cathode of the PEO process, respectively. The PEO coating was carried out on a circular area with a diameter of 6 mm on the (100) plane of the NSA under a high direct current (DC) pulse voltage in an electrolytic solution kept at 20^{o}C. The pulse voltage was applied between the anode and cathode with a bipolar DC power generator (HSA4052, NF Co., Ltd.) and a function generator (SG-4105, Iwatsu Co., Ltd.). The maximum voltage of the pulses with a duty ratio of 10% and the frequency of 1 kHz was varied from 100 V to 250 V. A two-step PEO process was used to make the OBC and TBC. In the first step to make the OBC, the coated NSA was oxidized with spark discharges at 250 V for 15 min in 0.25 mol/L of $Na_4P_2O_7$ solution. In the second step to make the TBC, the NSA covered with the OBC was oxidized at 100 V for a couple of minutes in 2.54 mol/L of $K_2[Zr(CO_3)_2(OH)_2]$ solution.

2.2. Characterization of PEO coating

X-ray diffraction (XRD) (RINT2000, Rigaku Co., Ltd.) was used to examine the crystalline phases of the OBC and TBC. XRD was carried out using the CuKα line and scanning from 20^o to 70^o in 2θ at a rate of 1^o/min. The microstructure of the coating was observed with FE-SEM (SP4500, Hitachi High Technology Co., Ltd.). The chemical composition of the coating was mapped with energy dispersive x-ray spectroscopy (EDS) equipment mounted on the SEM. The bond strength between the PEO coating and NSA substrate was measured with a testing machine (AG-100KNG, Shimadzu Co., Ltd.) by using an apparatus designed to apply a tensile load perpendicularly to the interface between the coating and substrate. The tensile test was carried out at a loading rate of 1 mm/min. The bond strength was measured in a circle with a diameter of 6 mm where a rod was connected with glue and was pulled to separate the coating from the substrate. The number of the measurements was five. The thermal conductivity of the PEO coating was measured with the laser flash method (TC-9000, Ulvac-Riko Inc.).

3. Results and discussion

3.1. Microstructural characterization of coatings on NSA

Figure 1 shows an SEM cross section of the NSA coated with OBC. The elemental distributions of Ni, Al, and O in the coating, as measured by EDS, are superimposed on

it. Although this OBC may be too thin to suppress the oxidation of the NSA, it could be made thicker by changing the PEO conditions, for example, by increasing the PEO voltage and/or duration.

The figure shows that there is an Al-rich NSA (ANSA) structure with three different layers:

(1) A continuous textured layer with a thickness of about 3 μm next to the NSA,

(2) A layer with a lot of acicular grains in the matrix,

(3) A layer with a few acicular grains next to the OBC.

The atomic ratio of Ni to Al measured with EDS and the phase diagram of Al and Ni led us to suppose that the first, second, and third layers respectively consist of a Ni-based solid solution including Al+Ni_3Al, Ni_2Al_3+$NiAl_3$, and a $NiAl_3$+Al based solid solution including Ni. Ni_3Al phase precipitated in a conventional TBC is known to increase the oxidation resistance of the NSA [25]. To increase the oxidation resistance and stability of the TBC coated NSA at elevated temperatures, the thickness of the layer containing Ni_3Al can be increased and the thickness of the Al-based solid solution layer can be decreased by varying the PEO conditions.

Figure 2 shows an SEM cross section of the NSA coated with TBC and OBC. The thickness of TBC is about 50 μm as a result of PEO for 15 minutes. The elemental

distributions of Ni, Al, O, and Zr in the coatings, as measured by EDS, are superimposed on it. The XRD profile shown in Fig. 3 indicates that the TBC consisted of monoclinic- ZrO_2 as well as high temperature ZrO_2 phase such as tetragonal- and/or cubic. The TBC formed rapidly at locally elevated temperatures caused by the spark discharge because tetragonal- and cubic-ZrO_2 are thermodynamically stable above 1170 and 2370^{o}C, respectively.

The TBC had a unique gradient porous texture, characterized by there being relatively large pores near the interface between the OBC and TBC and fewer and smaller pores farther from the interface (See Fig. 4: TBC top surface (a) and the inside of TBC at a distance of 35 μm (b) and 10 μm (c) from the OBC). An image analysis was carried out on the pores on each surface to evaluate the porosity of coating. The coating porosity was evaluated with the area ratio of pores observed with SEM. The gradient porous texture was attributed to the change in the growth mechanism of the TBC during the PEO process. Figure 5 shows the change in the current of the PEO circuit during the TBC. The current in Fig.5 was evaluated with averaging fluctuated current in every one second in order to check a comprehensive change in the current during PEO. In the first stage, the current increases almost linearly with time, and Al_2O_3 forms on the OBC coated NSA gradually through the following electrochemical processes [26],

$$2[Al(OH)_4]^- + 2H^+ + (n-5)H_2O \rightarrow Al_2O_3 + n\,H_2O \quad (1)$$

$$2Al + 9H_2O \rightarrow Al_2O_3 + 6H_3O^+ + 6e^- \quad (2)$$

In the second stage, where the current is very large, the TBC grows rapidly and breakdown with the spark discharges make large holes in it. This is why relatively large pores are observed near the interface between the OBC and TBC. The electrochemical reaction on the anode for incorporating Zr^{4+} ions from the electrolyte into the TBC is as follows:

$$5[Zr(CO_3)_2(OH)_2]^{2-} \rightarrow 5ZrO_2 + 10CO_2\uparrow + 10H_2O + 10e^- \quad (3)$$

A glow discharge [27, 28] may describe coating mechanism in the final stage of PEO process after the rapid TBC growth with spark discharges, in which the current gradually decreases as the PEO progresses and lights with small intensity are actually observed on the anode surface. The transition from spark to glow discharge occurs when the thickness of TBC exceeds a certain value, because higher voltage applied between the anode and cathode is required to continue breakdown through a thick TBC with a spark discharge [3]. The energy density of the glow discharge observed on the TBC surface seemed to be too small for it to make a hole through the TBC. Porous ZrO_2 may be spattered by the glow discharge on the porous TBC. As a result, the large holes made by spark discharge get plugged up by the ZrO_2 deposited during the glow discharge. The

plugging may help to prevent oxygen transport from the ambient to the NSA through the porous TBC.

Figure 6 shows the very fine microstructure of the ZrO_2 grains with a diameter of 300 nm in the TBC. This structure can be obviously attributed to quenching caused by the rapid heating of the discharge followed by cooling in the electrolytic solution. The quenching rate of the PEO process was estimated to be about 10^7 K/sec [28].

3.2. Thermal conductivity of PEO coating on NSA substrate

The thermal diffusivity α of the NSA with the TBC was measured with the laser flash method. A bilayer model was used to estimate the α-value of the coating [29]. The boundary of the bilayer was assumed to be between the OBC and ANSA, which means that the thermal diffusivity would be estimated for a PEO coating consisting of the OBC and TBC. Accordingly, the thermal diffusivities of the PEO coating and NSA with ANSA were estimated to be $4.26\pm1.87\times10^{-7}$ and $3.69\pm0.05\times10^{-6}$ m^2/sec, respectively. The rather large deviation in the α value of the PEO coating is attributed to the variation in the thickness of the PEO coating and ANSA.

The thermal conductivity K of the PEO coating is estimated to be 1.06 W/mK for a specific heat capacity c of 0.472 J/gK and 1.03 W/mK for 0.460 J/gK. These

conductivities are smaller than that of TBCs made with EB-PVD (1.575 W/mK with an α of 8.30×10^{-7} m^2/sec and a c of 0.460 J/gK [30]) and larger than that of TBC made with APS (0.537 W/mK with an α of 2.78×10^{-7} m^2/sec and a c of 0.472 J/gK) [30]. The lower value of K of the TBC made with APS owes to the low density of the coating (4.10 g/cm^3), whereas the apparent density of the PEO coating is 5.28 g/cm^3 with an average porosity of 11.6%. TBC made with EB-PVD has a rather high thermal conductivity regardless of its low density (4.13 g/cm^3) because of its fibrous open pores and unique segmented columnar structure [30]. The thermal conductivity of a porous material with fibrous open pores in the longitudinal direction of the pore, K_{op}, is approximately calculated as follows [31]:

$$\frac{K_{op}}{K_s} = (1-P) + P\frac{K_g}{K_s} \qquad (4)$$

where P is porosity, and K_s and K_g are the thermal conductivities of solid and gas, respectively. The thermal conductivity of a porous material with closed pores, K_{cp}, is [12],

$$\frac{K_{cp}}{K_s} = \frac{1}{\left(1-P^{1/3}\right) + \dfrac{P^{1/3}}{\left(1-P^{2/3}\right) + P^{2/3}\dfrac{K_g}{K_s}}} \qquad (5)$$

Figure 7 plots the specific thermal conductivities, K_{op}/K_s and K_{cp}/K_s, for a K_g of 0.03697W/mK for air at room temperature. This plot indicates that K_{cp} is smaller than

K_{op} at the same porosity. The TBC made with the PEO technique has a lower thermal conductivity than that of the TBC made with EB-PVD, because the pores in the TBC made with PEO are plugged by the glow discharge. Moreover, the porosity of the TBC made with PEO could have been underestimated in the SEM image analysis of the pores and the very fine microstructure is characterized by the fine ZrO_2 grains (Fig. 6). In addition to the porous texture with closed pores, these could also explain why the K of the TBC made with PEO is lower than that of the TBC made with EB-PVD.

3.3. Bond strength between PEO coating and NSA substrate

The bond strength between the PEO coating and NSA substrate was measured to be 28.8±4.8 MPa. On the other hand, the bond strength between the TBC made with APS and NSA substrate is reported to be 32.8±4.4 MPa [32]. The former bond strength is somewhat smaller than the latter, but they are more or less comparable. Figure 8 shows an SEM image of the fractured surface. The image has dark parts (for example, A in Fig. 8) and bright parts (for example, B in Fig. 8). EDS on the dark parts revealed a remarkably large peak that could be assigned to aluminum (Fig. 9). EDS on the bright parts revealed a significantly large peak that could be assigned to zirconium. In the bonding strength test, the PEO coated NSA often fractured at the interface between the

OBC and TBC. As described above, there are large pores near the interface owing to the spark discharge. The large pores must be the origin of fractures and determine the bond strength.

4. Conclusions

TBCs made of porous ZrO_2 based ceramic were created by performing PEO on NSA in a $K_2[Zr(CO_3)_2(OH)_2]$ solution. The TBC has a gradient porous texture in which there are large pores near the interface between the OBC and TBC and the number and size of pores in TBC decrease with increasing distance from the interface. The fine structure of the TBC consisted of ZrO_2 grains with a diameter of about 300 nm. The gradient porous structure with fine grains is due to the spark and glow discharge during PEO process, and it leads to a thermal conductivity of about 1 W/mK (equivalent to that of conventional TBC) . The bond strength between the PEO coatings and substrate was 26.8±6.6 MPa, which is almost equivalent to that of conventional TBCs. During the bonding strength test, the PEO coated NSA often fractured at the interface between the OBC and TBC with large pores.

Acknowledgements

Financial support for this research was provided by a Grant-in-Aid for Challenging Exploratory Research (No. 21656184).

References

[1] E. Demaray, DOE contract DE-AC06-76 (1982) RL01830.
[2] P. Meyer, S. Muehlberger, Thin Solid Films 118 (1984) 445-456.
[3] A.L. Yelokhin, X. Nie, A. Leyland, A. Mathews, S.J. Dowey, Surf. Coat. Technol. 122 (1999) 73-93.
[4] T. Akatsu, T. Kato, Y. Shinoda, F. Wakai, IOP series: Mater. Sci. Eng. 18 (2011) 202005.
[5] Z.P. Yao, H.H. Gao, Z.H. Jiang, F.P. Wang, J. Am. Ceram. Soc. 91 (2008) 555-558.
[6] H.H. Luo, Q.Z. Cai, B.K. Wei, B. Yu, J. He, J. Alloys Compd. 474 (2009) 551-556.
[7] J. Liang, P. Bala Srinivasan, C. Blawert, W. Dietzel, Corros. Sci. 51 (2009) 2483-2492.
[8] J. Liang, P. Bala Srinivasan, C. Blawert, W. Dietzel, Corros. Sci. 52 (2010) 540-547.
[9] H.H. Luo, Q.Z. Cai, J. He, B.K. Wei, Curr. Appl. Phys. 9 (2009) 1341-1346.
[10] Y. Han, J.F. Song, J. Am. Ceram. Soc., 92 (2009) 1813-1816.
[11] W. Mu, Y. Han, Surf. Coat. Technol. 202 (2008) 4278-4284.
[12] F. Liu, D.Y. Shan, Y.W. Song, E.H. Han, Trans. Nonferrous Met. Soc. China 21 (2011) 943-949.
[13] Z. Wu, Z. Yao, Z. Jiang, Rare Metals 27 (2008) 55-58.
[14] Z. Wu, Z. Yao, F. Jia, Z. Jiang, Adv. Mater. Res. 105-106 (2010) 505-508.
[15] Z. Wu, Z. Jiang, Z. Yao, X. Zhang, J. Inorg. Mater. 22 (2007) 555-559.
[16] E. Matykina, R. Arrabal, P. Skeldon, G.E. Thompson, J. Appl. Electrochem. 38 (2008) 1357-1383.
[17] E. Matykina, R. Arrabal, F. Monfort, P. Skeldon, G.E. Thompson, Appl. Surf. Sci. 255 (2008) 2830-2839.
[18] S.G. Xin, R.G. Zhao, H. Dou, L.X. Song, J. Inorg. Mater. 24 (2009) 107-110.
[19] X.M. Zhang, D.F. Chen, X.Z. Gong, S.Q. Yang, X.B. Tian, J. Inorg. Mater. 25 (2010) 865-870.
[20] P. Bala Srinivasan, J. Liang, C. Blawert, W. Dietzel, Appl. Surf. Sci. 256 (2010) 3265-3273.
[21] F. Liu, D.Y. Shan, Y.W. Song, E.H. Han, W. Ke, Corros. Sci. 53 (2011) 3845-3852.
[22] M. Tang, W. Li, H. Liu, L. Zhu, Appl. Surf. Sci. 258 (2012) 5869-5875.

[23] V.S. Rudnev, I.V. Malyshev, I.V. Lukiyanchuk, V.G. Kuryavyi, Protec. Metals Phys. Chem. Surf. 48 (2012) 455-461.
[24] V. Shoaei-Rad, M.R. Bayati, H.R. Zargar, J. Javadpour, F. Golestani-Fard, Mater. Res. Bull. 47 (2012) 1494-1499.
[25] S. Bose, High Temperature Coatings, Butterworth–Heinemann (2007) 155-226.
[26] L.O. Snizhko, A.L. Yerokhin, N.L. Gurevina, V.A. Patalakha, A. Matthews, Thin Solid Films 516 (2007) 460-464.
[27] A. Hickling, M. D. Ingram, Trans. Faraday Soc. 60 (1964) 783.
[28] A. L. Yerokhin, L.O. Snizhko, N.L. Gurevina, A. Leyland, A. Pilkington. A. Matthews, J. Phys. D: Appl. Phys. 36 (2003) 2110-2120.
[29] N. Araki, A. Makino, J. Mihara, The Ninth Japan Symposium on Thermophysical Properties (1988) 179-182
[30] P. Scardi, M. Leoni, J. Am. Ceram. Soc., 84 (2001) 827-835
[31] R. Kondo, "Porous material – The nature and use –", Gihoudou Publishing Co., Ltd., (1975) 186-188.
[32] M. Okazaki et al, Soc. Mater. Sci. Jpn 52 (2003) 53.

Figure captions

Fig. 1. SEM image of cross section of NSA coated with OBC. Elemental distributions of Ni, Al, and O measured with EDS are superimposed on the SEM image.

Fig. 2. SEM image of cross section of NSA coated with TBC on OBC. Elemental distributions of Ni, Al, O and Zr measured with EDS are superimposed on the SEM image.

Fig. 3. XRD profile of TBC.

Fig. 4. Porous texture of TBC: SEM images of the TBC top surface (a), the inside of the TBC at a distance of 35 μm from the OBC (b), and the inside at a distance of 10 μm from the OBC (c).

Fig. 5. Current flowing in the PEO circuit during the process.

Fig. 6. SEM images of TBC microstructure with fine ZrO_2 grains (diameter: 300 nm): cross section (a) and on the surface (b).

Fig. 7. Specific thermal conductivity of a material with fibrous open or closed pores calculated as a function of porosity. Solid lines denote the thermal conductivities in the longitudinal direction of a material with fibrous open pores, and dotted lines denote the thermal conductivities of materials with closed pores in the longitudinal direction of the pore.

Fig. 8. Surface fractured in bonding strength test, as observed by SEM. The fractured surface has dark (A in Fig. 8) and bright (B in Fig. 8) parts.

Fig. 9. EDS on a surface that fractured in the bonding strength test. The broken line is for EDS on A in Fig. 8, and the solid lines are for EDS on B in Fig. 8.

Fig. 1.

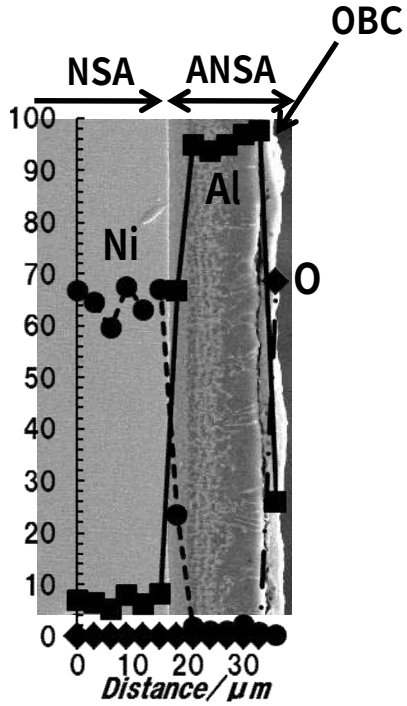
OBC
NSA
ANSA
100
90
80
70
60
50
40
30
20
10
0
Ni
Al
O
0
10
20
30
Distance/μm

Fig. 2.

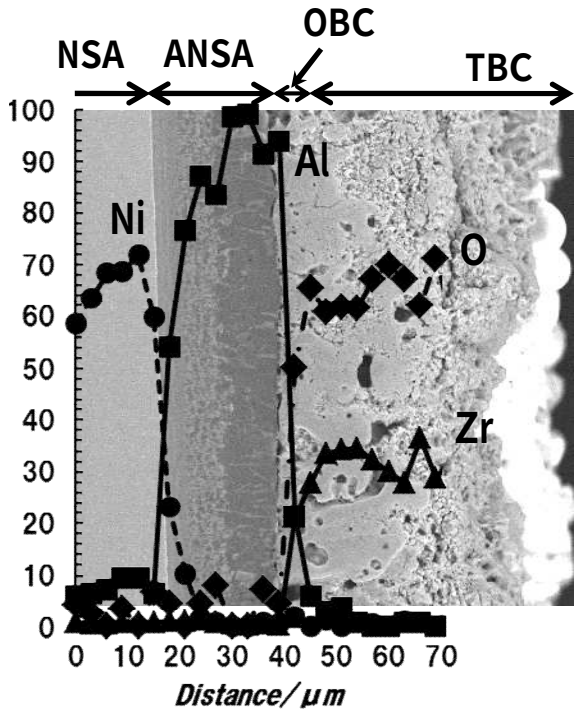
NSA
ANSA
OBC
TBC
Ni
Al
O
Zr
100
90
80
70
60
50
40
30
20
10
0
0 10 20 30 40 50 60 70
Distance/μm

Fig. 3.

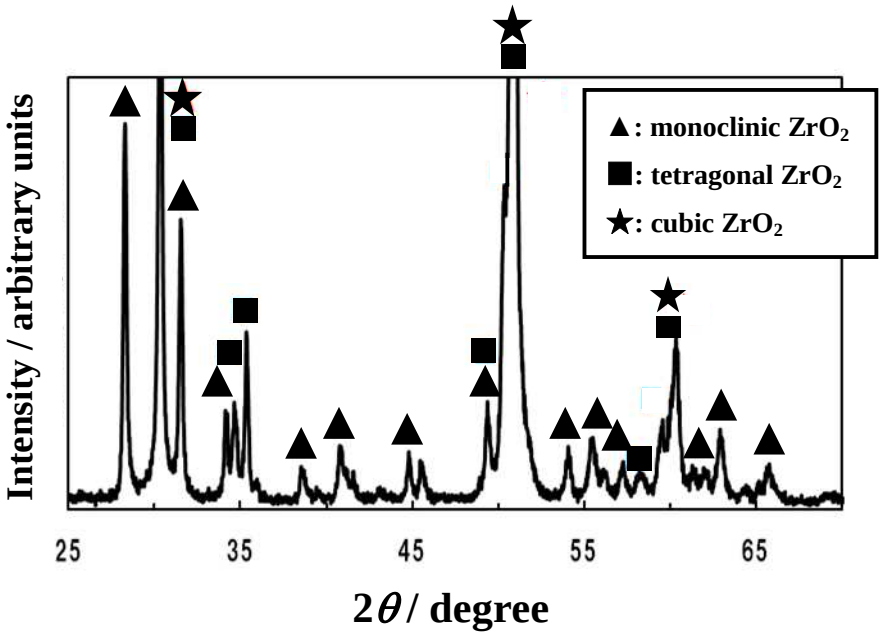
▲: monoclinic ZrO2
■: tetragonal ZrO2
★: cubic ZrO2
Intensity / arbitrary units
25
35
45
55
65
2θ / degree

Fig. 4.

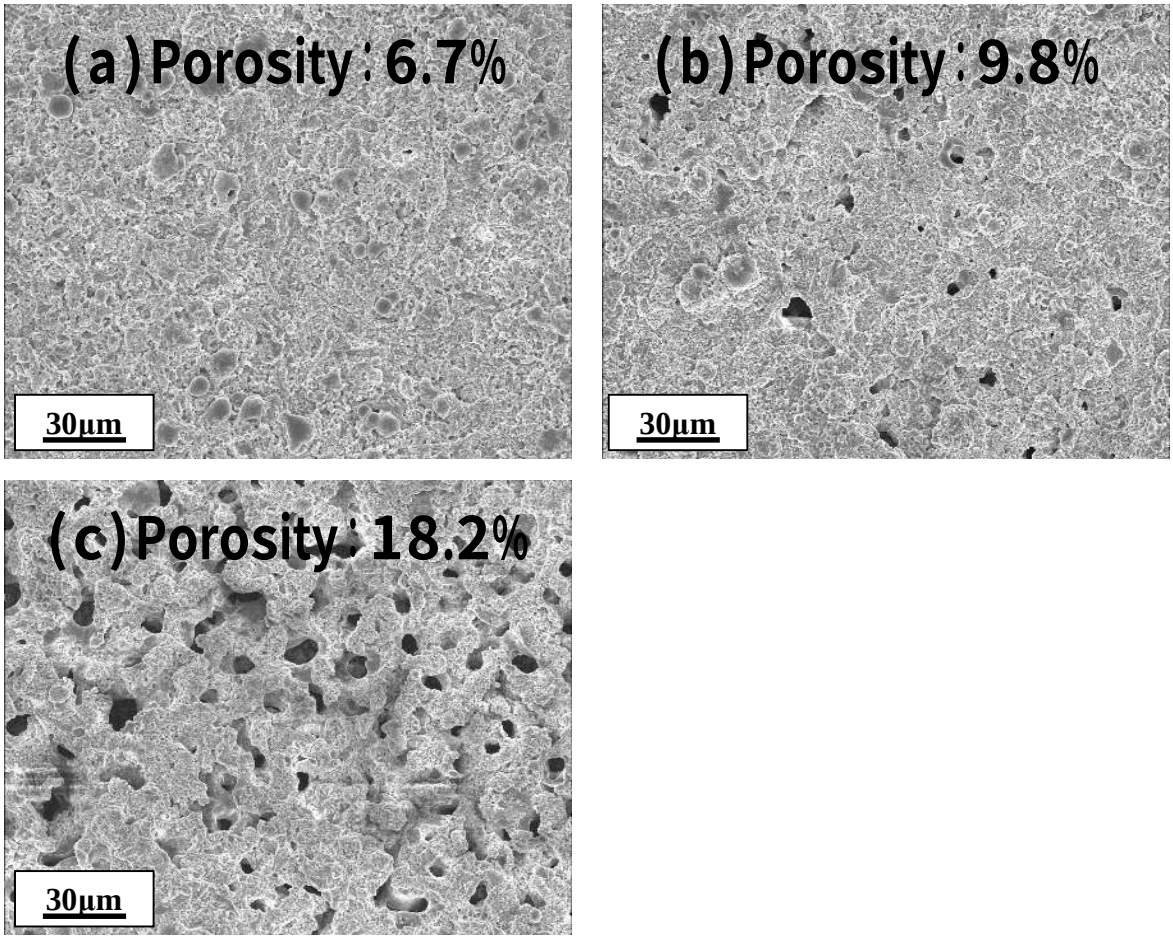

Fig. 5.

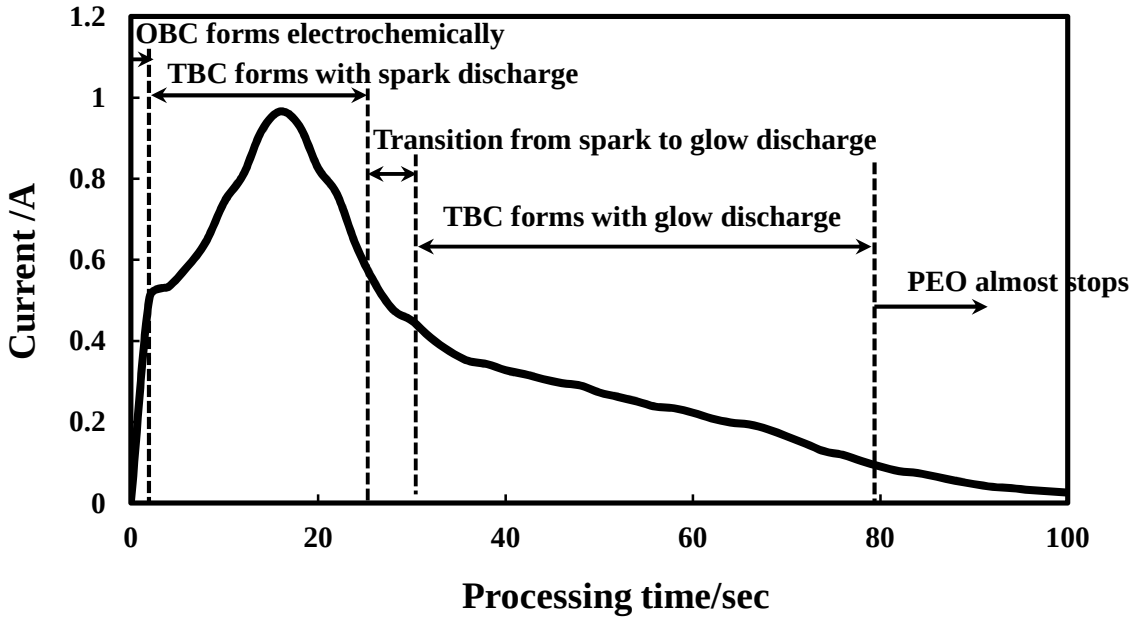
OBC forms electrochemically
TBC forms with spark discharge
Transition from spark to glow discharge
TBC forms with glow discharge
PEO almost stops
Current /A
Processing time/sec
1.2
1
0.8
0.6
0.4
0.2
0
0
20
40
60
80
100

Fig. 6.

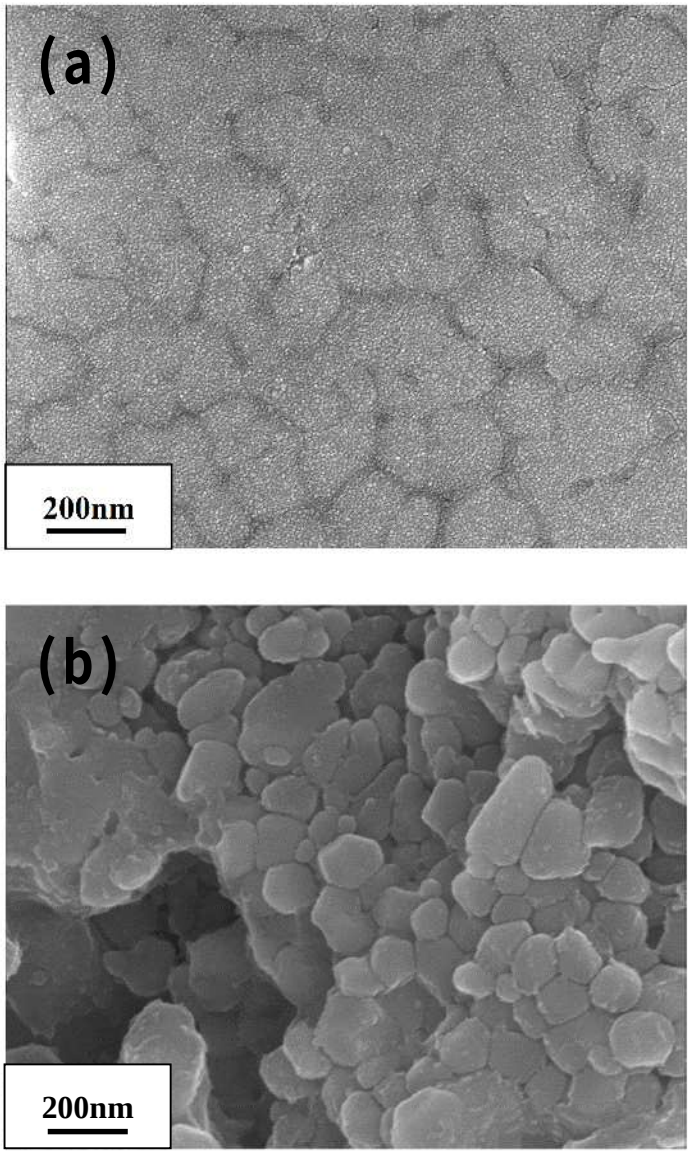

Fig. 7.

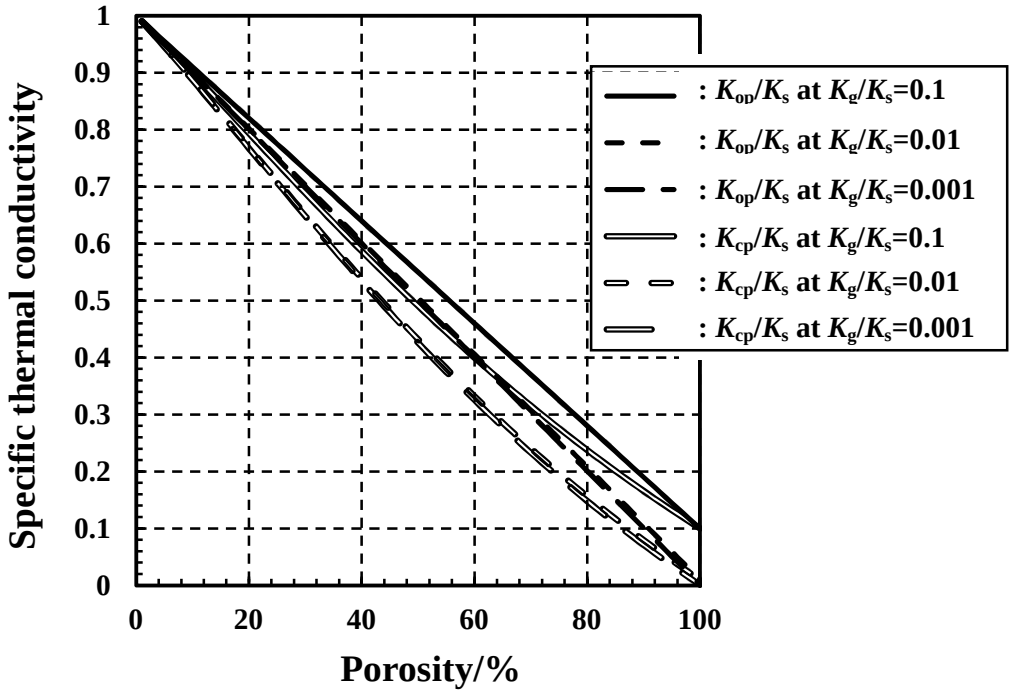
Specific thermal conductivity
1
0.9
0.8
0.7
0.6
0.5
0.4
0.3
0.2
0.1
0
0
20
40
60
80
100
Porosity/%
: K_{op}/K_s at K_g/K_s=0.1
: K_{op}/K_s at K_g/K_s=0.01
: K_{op}/K_s at K_g/K_s=0.001
: K_{cp}/K_s at K_g/K_s=0.1
: K_{cp}/K_s at K_g/K_s=0.01
: K_{cp}/K_s at K_g/K_s=0.001

Fig. 8.

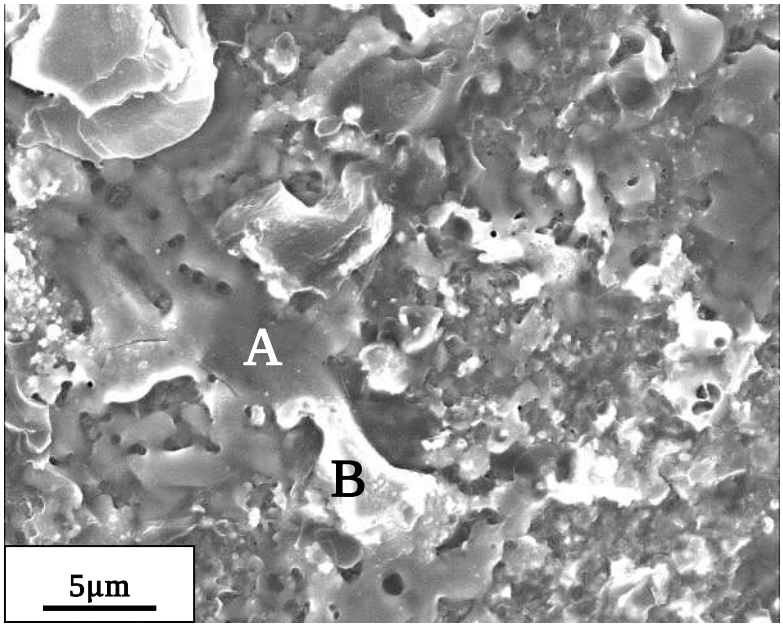

Fig. 9.

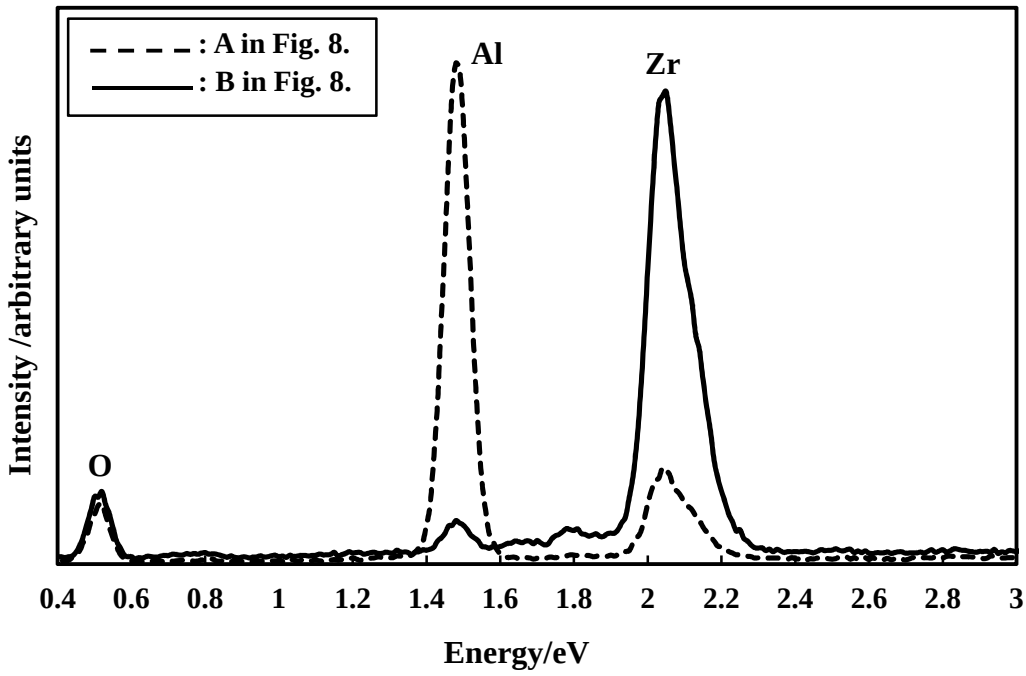
: A in Fig. 8.
: B in Fig. 8.
Al
Zr
O
Intensity /arbitrary units
0.4
0.6
0.8
1
1.2
1.4
1.6
1.8
2
2.2
2.4
2.6
2.8
3
Energy/eV